Structural insights into mis-regulation of protein kinase A in human tumors

Jonah Cheung[a,1], Christopher Ginter[a], Michael Cassidy[a], Matthew C. Franklin[a], Michael J. Rudolph[a], Nicolas Robine[b], Robert B. Darnell[b,c,d], and Wayne A. Hendrickson[a,e,1]

[a]New York Structural Biology Center, New York, NY 10027; [b]New York Genome Center, New York, NY 10013; [c]Howard Hughes Medical Institute and [d]Laboratory of Molecular Neuro-Oncology, The Rockefeller University, New York, NY 10021; and [e]Department of Biochemistry and Molecular Biophysics, Columbia University, New York, NY 10032

Contributed by Wayne A. Hendrickson, December 18, 2014 (sent for review November 2, 2014; reviewed by Carlo M. Croce and John Kuriyan)

The extensively studied cAMP-dependent protein kinase A (PKA) is involved in the regulation of critical cell processes, including metabolism, gene expression, and cell proliferation; consequentially, mis-regulation of PKA signaling is implicated in tumorigenesis. Recent genomic studies have identified recurrent mutations in the catalytic subunit of PKA in tumors associated with Cushing's syndrome, a kidney disorder leading to excessive cortisol production, and also in tumors associated with fibrolamellar hepatocellular carcinoma (FL-HCC), a rare liver cancer. Expression of a L205R point mutant and a DnaJ–PKA fusion protein were found to be linked to Cushing's syndrome and FL-HCC, respectively. Here we reveal contrasting mechanisms for increased PKA signaling at the molecular level through structural determination and biochemical characterization of the aberrant enzymes. In the Cushing's syndrome disorder, we find that the L205R mutation abolishes regulatory-subunit binding, leading to constitutive, cAMP-independent signaling. In FL-HCC, the DnaJ–PKA chimera remains under regulatory subunit control; however, its overexpression from the DnaJ promoter leads to enhanced cAMP-dependent signaling. Our findings provide a structural understanding of the two distinct disease mechanisms and they offer a basis for designing effective drugs for their treatment.

cancer mutations | Cushing's syndrome | fibrolamelllar hepatocellular carcinoma | chimeric protein

Quiescent protein kinase A (PKA) exists as a heterotetramer of two catalytic (C) subunits bound in an inactivated state to a dimer of two regulatory (R) subunits. Each R subunit contains a flexible inhibitory segment that binds in an extended conformation along the active-site cleft in the C subunit, where it limits catalytic activity by blocking access to the active site (1). Upon binding of the second messenger cAMP to the R subunits, the C subunits are released, enabling them to phosphorylate downstream protein targets and affect cellular functions (2). Four isoforms of the R subunit (RIα, RIβ, RIIα, and RIIβ) are known. Structures of the R_2:C_2 holoenzyme provide insight into mechanisms of allosteric control and reveal distinct, isoform-specific assemblies of the tetramers (3–6), even though all R:C heterodimer associations are similar. Specificity of PKA activity is also controlled by localization. Type I PKAs are generally cytoplasmic, whereas type II PKAs may be localized to membranes and subcellular structures through attachment to anchoring proteins (7).

Sequencing efforts have identified somatic mutations in the PKA catalytic-subunit gene (*PRKACA*) in tissues associated with two different disease states. In Cushing's syndrome, a disorder arising from overproduction of cortisol from tumors and hyperplasia of the adrenal cortex, mutations in *PRKACA* have been discovered in tumor specimens from patients with this disease (8–11), including the predominant L205R mutation in the PKA C subunit. In fibrolamellar hepatocellular carcinoma (FL-HCC), a rare liver tumor affecting young adults, ∼400-kb deletions have been discovered in chromosome 19. These deletions result in fusions of the gene for the molecular chaperone DnaJ (*DnaJB1*) with *PRKACA* to produce a predominant chimeric protein derived from exon 1 of *DnaJB1* fused to exon 2 of *PRKACA* (12, 13). Both sets of studies similarly postulated that these mutations lead to mis-regulation of signaling by affecting R-subunit binding. The Cushing's syndrome studies proposed a mechanism based on modeling of the mutation, and the FL-HCC studies stated presumptions that were not validated experimentally. Through structural and biochemical analysis of the mutant PKA catalytic subunits, we reveal contrasting mechanisms of disease at the molecular level.

Results and Discussion

Summary of Crystal Structures. Four structures of human PKA C subunits were determined here (Fig. 1, Table 1, and Table S1): the full-length wild-type C subunit (PKAc), the predominant point mutant (PKAc L205R), the predominant chimeric fusion protein (DnaJ–PKAc), and PKAc with exon 1 residues deleted (PKAc Δexon1). All structures were determined as complexes with ATP and the protein kinase inhibitor (PKI) peptide (5–24). In each, ATP is bound with two metal ions within the cleft formed between the smaller N-terminal and larger C-terminal lobes of the C subunit, associated as previously described (14). The peptide is bound within the cleft and also forms an amphipathic N-terminal helix laid against the surface of the large lobe. All residues of PKAc Δexon1 are ordered, beginning at residue 15, which corresponds to the start of *PRKACA* exon 2. The deletion of residues encoded by exon 1 does not appear to

Significance

Mutations in the catalytic subunit of protein kinase A (PKA) have been found in tumors associated with the kidney disorder Cushing's syndrome and with the rare liver cancer fibrolamellar hepatocellular carcinoma (FL-HCC). Crystal structures and biochemical characterizations of the relevant PKA mutants clarify the molecular basis for disease caused by these mutations. We find contrasting underlying mechanisms for increased PKA signaling in these cancers. In Cushing's syndrome, the L205R PKA mutation abolishes regulatory-subunit binding, whereas in FL-HCC, the recurring DnaJ–PKA fusion that results from a chromosomal deletion exhibits wild-type characteristics, but is overproduced by a more active promoter. Our findings provide a structural basis for designing selective drugs that may lead to effective treatments for these diseases.

Author contributions: J.C., M.C.F., M.J.R., R.B.D., and W.A.H. designed research; J.C., C.G., and M.C. performed research; J.C., N.R., and W.A.H. analyzed data; and J.C. and W.A.H. wrote the paper.

Reviewers: C.M.C., The Ohio State University; and J.K., University of California, Berkeley.

The authors declare no conflict of interest.

Database deposition: The atomic coordinates and structure factors have been deposited in the Protein Data Bank, www.pdb.org (PDB ID codes 4WB5, 4WB6, 4WB7, and 4WB8).

[1]To whom correspondence may be addressed. Email: jcheung@nysbc.org or wayne@xtl.cumc.columbia.edu.

This article contains supporting information online at www.pnas.org/lookup/suppl/doi:10.1073/pnas.1424206112/-/DCSupplemental.

Downloaded from https://www.pnas.org by 174.168.116.9 on January 19, 2024 from IP address 174.168.116.9.

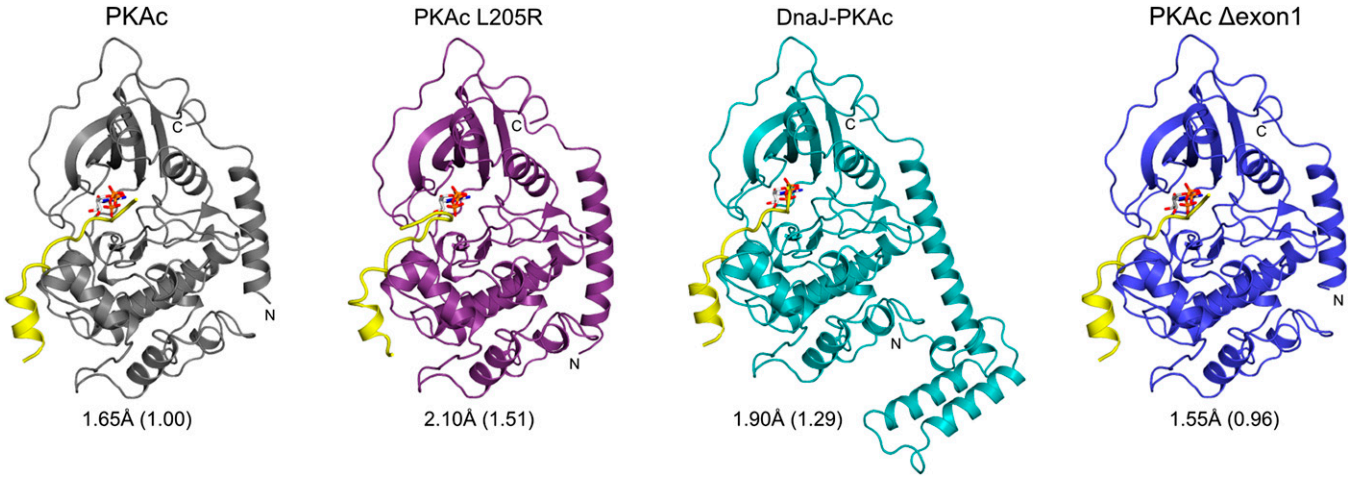

Fig. 1. Structures of wild-type and tumor-related human PKA. Structures are drawn in ribbon representations for the four designated catalytic subunit constructs, each in complex with ATP and PKI inhibitor peptide. Corresponding resolution limits and relative activities (in parenthesis) are listed below (for activity measurements, see Fig. S1). In each representation, PKI is colored yellow and ATP is drawn in stick representation with carbon, nitrogen, oxygen, and phosphorous atoms colored white, blue, red, and orange, respectively.

destabilize PKAc nor does it appear to affect kinase activity significantly (Fig. S1). In PKAc, the first 12 residues are disordered, as observed as well for the N-terminal segment of nonmyristoylated PKA C subunits (15). Because of crystal packing interactions in PKAc L205R, ordering begins at position 8 in this structure. All residues of the DnaJ–PKAc chimeric fusion protein are ordered.

Structural Basis for Abolished Regulatory Subunit Binding by PKAc L205R in Cushing's Syndrome. When the structures of PKAc and PKAc L205R are superimposed (Fig. 2 *A* and *B*), it is immediately clear that PKI is bound differently in the vicinity of R205. In the structure of PKAc, binding of PKI is as seen before (16) in an extended conformation along the active-site cleft with the side-chain of A21 (P0) pointing toward the γ-phosphate of ATP located 3.7 Å away. Protein-peptide contacts include ionic interactions between PKI arginine side-chains at positions 15 (P−6), 18 (P−3), and 19 (P−2) with a cluster of PKAc glutamate side-chains (positions 170, 203, 230), van der Waals contacts between the side-chains of PKI H23 (P+2) and PKAc F187 and L82, and a hydrogen bond between the side-chains of the C-terminal D24 (P+3) of PKI and K83 of PKAc. When complexed with the mutant, PKI residues at positions 22–24 turn away from the cleft, stabilized by an intramolecular hydrogen bond between the side-chains of R15 and H23 of PKI, van der Waals contacts between H23 of PKI and P202 of PKAc L205R, and a hydrogen bond between the C-terminal carboxylate of PKI with the carbonyl of D241 in the large lobe of PKA L205R. Minor differences in the conformation of PKI at the N terminus are caused by crystal packing interactions. The protrusion of the R205 side-chain into the cleft places it a mere 0.6 Å away from I22 (P+1) of PKI in its complex with PKAc. This steric clash is averted with PKI binding in the energetically more favorable conformation observed.

Previous studies (8–11) have suggested that the mutation may abolish the binding of PKAc L205R to the R subunit. The structure of PKAc L205R provides an atomic basis for this effect, where steric clash between R205 and the P+1 residue of the regulatory subunit inhibitory sequence is expected (Fig. 2*C*). Through gel-filtration experiments with purified RIα and RIIβ subunits, we show directly that the L205R mutation abolishes R subunit binding in solution (Fig. 3). Because the R:C interaction and regulation of catalytic activity depends upon binding of the R-subunit inhibitory segment with the C-subunit active-site cleft, the L205R mutation likely affects all isoforms in the same manner. Measurements of the intrinsic activities of purified C subunits (Fig. S1) also show elevated PKAc L205R activity, as previously reported (10, 11). Although it is not obvious how the mutation increases the catalytic rate, minor perturbations are observed in the packing of residues near the site of mutation and this may alter the dynamics of the protein in solution. The resulting up-regulation of PKA signaling, stemming both from loss of cAMP-dependent regulatory control and elevated catalytic rate caused by the mutation, represents a key molecular mechanism in the formation of adenomas and hyperplasia in the adrenal cortex leading to Cushing's syndrome.

Retention of Regulatory Subunit Binding by the DnaJ–PKAc Fusion Protein. In DnaJ–PKAc (Fig. 4*A*), the additional 69 residues from exon 1 of DnaJ add a subdomain containing the first four helices of DnaJ in place of the exon 1-encoded residues at the start of PKAc. The last three residues from DnaJ exon 1, which are part of a loop in a bacterial DnaJ homolog (17), form part of

Table 1. Summary of structures

Variable	PKAc	PKAc L205R	DnaJ–PKAc	PKAc Δexon1
d_{min} (Å)	1.65	2.10	1.90	1.55
Space group	$P2_12_12_1$	$P2_1$	$P2_12_12_1$	$P2_12_12_1$
Cell parameters: *a, b, c* (Å)	73.2, 75.1, 80.7	56.2, 90.2, 90.4 (β = 96.1°)	59.2, 121.2, 173.7	72.8, 75.9, 80.6
$R^*/R_{free}^{\dagger}$ (%)	16.3 (19.6)	18.8 (23.7)	15.0 (18.8)	16.3 (18.4)
PDB ID code	4WB5	4WB6	4WB7	4WB8

*$R = \sum ||F_o| - |F_c|| / \sum |F_o|$, where F_o and F_c denote observe and calculated structure factors, respectively.
†R_{free} was calculated using 5% of data excluded from refinement.

Downloaded from https://www.pnas.org by 174.168.116.9 on January 19, 2024 from IP address 174.168.116.9.

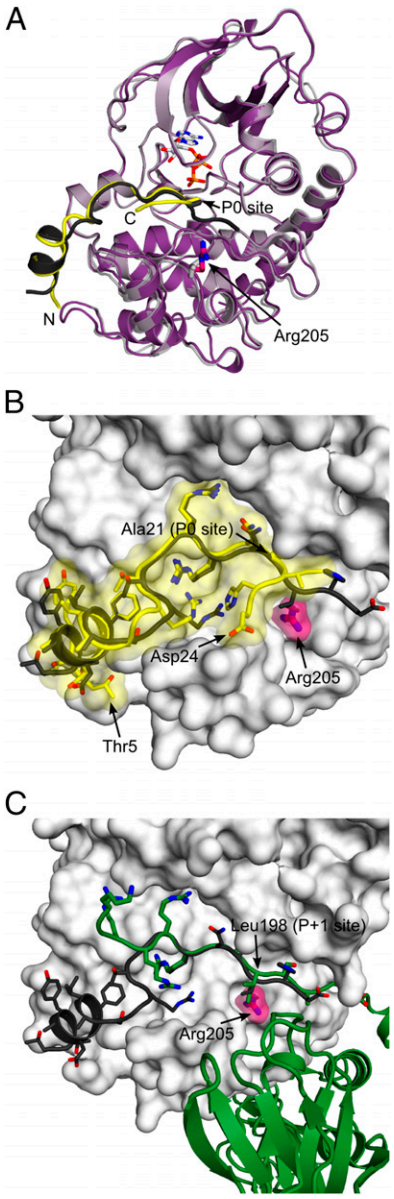

Fig. 2. Structural analysis of PKAc L205R. (*A*) Ribbon drawings of PKAc (gray) and PKAc L205R (purple) structures superimposed with corresponding bound PKIs colored black and yellow, respectively. The bound ATP (drawn for PKAc L205R only) and the side-chains of residue 205 for both structures are drawn as sticks. The pseudosubstrate P0 position of PKI is indicated. (*B*) An expanded view of the PKAc binding cleft. The molecular surfaces of PKAc, and PKI and Arg205 in the superimposed mutant are drawn in gray, semitransparent yellow, and semitransparent magenta, respectively. The peptide backbone and side-chains of PKI in the wild-type and mutant structures are shown as ribbons and sticks. The atomic colorings are carbon (black for wild-type associated and yellow for L205R associated), oxygen (red) and nitrogen (blue). (*C*) The binding of RIα in the PKAc binding cleft. Based on the structure of the PKA holoenzyme (PDB ID code 2QCS) (41), a model of RIα (green) bound to PKAc (gray surface) is drawn, showing the binding of the RIα inhibitory sequence (side-chains drawn and colored by atom) within the cleft with respect to Arg205 (same depiction as in *B*) of the superimposed mutant.

a continuous helix in DnaJ–PKAc. The relative orientation of the four helices in exon 1 of DnaJ is not altered significantly in the fusion, and the N terminus is partially buried against the large lobe. Average B-factors in the DnaJ moiety are higher than the rest of the protein (59 $Å^2$ vs. 24 $Å^2$). A superimposition of DnaJ–PKAc and PKAc reveals that the corresponding N-terminal helix in PKAc which curves against the large lobe is more linear in the fusion. The conformation of bound PKI(5–24) is similar in both except for small differences at the C-terminal end, which is involved in crystal contacts in DnaJ–PKAc. The conformation of residues in the catalytic site and nucleotide-binding pocket are also similar, and ATP is bound in the same manner, except that Zn^{2+} has replaced Mg^{2+} in DnaJ–PKAc because of the relatively high zinc concentration used in crystallization. Additional zinc atoms are also seen in DnaJ–PKAc-mediating crystal contacts, but they do not appear to significantly perturb the structure.

In contrast to the Cushing's syndrome-associated mutant, and contrary to a conjecture that the N terminus of the PKA C subunit is involved in R subunit binding (12), surface plasmon resonance (SPR) experiments revealed that DnaJ–PKAc binds to type I and type II R subunits with similar binding kinetics and affinities as the wild-type (Fig. 4 *B* and *C* and Table S2). Gel-filtration analysis also showed that the residues derived from DnaJ do not disrupt formation of heterodimers or heterotetramers with purified R subunits in solution; the behavior of the DnaJ–PKAc fusion in solution is identical to that of the wild-type C subunit (Fig. S2). Modeling of a DnaJ–PKAc:RIα heterodimer (Fig. S3) suggests compatibility with R subunit binding. Thus, unlike previously believed, the underlying mechanism for mis-regulation of PKA signaling in FL-HCC appears very different from that in Cushing's syndrome.

Unlikelihood of PKAc Mis-Localization as a Disease Mechanism for FL-HCC. We further investigated possibilities that mis-regulation of PKA signaling is caused by mis-localization of the PKA fusion, a mechanism known to be associated with disease states (18). We did not expect interactions with canonical A-kinase anchoring proteins (AKAPs), which localize PKA through binding to the

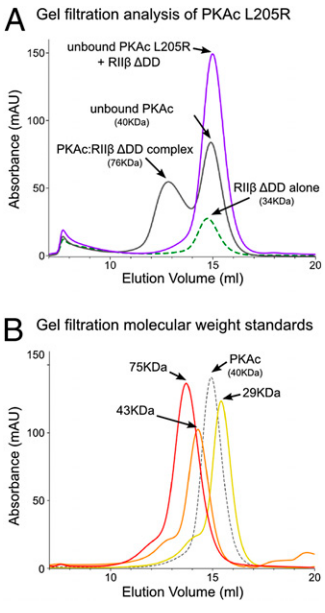

Fig. 3. Biophysical analysis of PKAc L205R. (*A*) Gel-filtration absorbance curves (λ = 280 nm) are shown for coinjections of RIIβ ΔDD with PKAc (gray), with PKAc L205R (purple), and alone (green), showing complex formation with PKAc but not PKAc L205R. Similar experiments performed with RIα ΔDD also showed no interaction with PKAc L205R. PKA proteins injected alone (omitted for clarity) eluted as single peaks at ~15 mL. (*B*) Curves of protein gel-filtration standards of molecular weights 29, 43, and 75 kDa (yellow, orange, and red traces, respectively), injected individually, are shown. The curve of PKAc injected alone is shown in dashed gray.

Downloaded from https://www.pnas.org by 174.168.116.9 on January 19, 2024 from IP address 174.168.116.9.

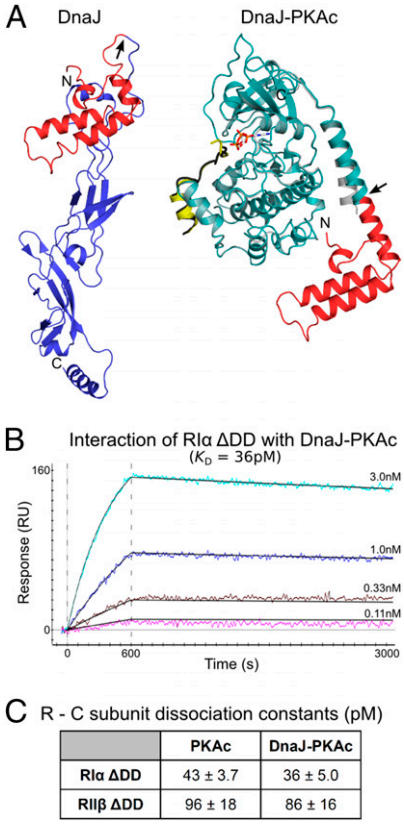

C R - C subunit dissociation constants (pM)

	PKAc	DnaJ-PKAc
RIα ΔDD	43 ± 3.7	36 ± 5.0
RIIβ ΔDD	96 ± 18	86 ± 16

Fig. 4. Structural and biophysical analysis of DnaJ–PKAc. (*A*) DnaJ structural comparisons. Ribbon drawings for the DnaJ homolog from *Thermus thermophilus* (PDB ID code 4J80) (*Left*) and DnaJ–PKAc (*Right*) are disposed with their J domains (red), which correspond to exon 1 of the human *DnaJB1* gene, in the same orientation. Apart from the J-domain coloring, DnaJ–PKAc is drawn as in Fig. 1 with its associated PKI (yellow) and ATP (colored sticks), but here superimposed upon PKAc (gray) with its PKI (black). The remainder of the bacterial DnaJ is colored blue. Arrows mark positions corresponding to the boundary following *DnaJB1* exons. (*B*) Representative SPR response curves for regulatory domain binding to DnaJ–PKAc. Colored traces are shown for various concentrations of RIα ΔDD injected through a sensor-chip channel containing ∼300 RU of immobilized DnaJ–PKAc. Dashed vertical lines define the start and stop of injection times. Black lines through the responses are fittings generated assuming a Langmuir 1:1 binding model from which the dissociation constant (K_D) was determined (mean K_D values were calculated from a pair of experiments performed at two different C subunit immobilization levels). (*C*) Matrix of dissociation values. K_D values for R-C subunit interactions were determined by SPR experiments as in *B*. Corresponding binding rate constants (k_a and k_d) are listed in Table S2. No significant differences were observed between between bindings to PKAc and DnaJ–PKAc.

N-terminal dimerization domain of R subunits (7), to be affected by the fusion because this region is readily accessible in the structures of PKA holoenzymes (3–6). AKIP1a, on the other hand, is an unconventional AKAP that binds to PKA near the N terminus of the C subunit (19). Because AKIP1a is involved with nuclear translocation of PKA and localization of PKA to NF-κB signaling complexes in the cytoplasm (19, 20), it did seem a candidate for fusion-affected mis-localization; however, we found that AKIP1a interaction with PKA is also preserved with DnaJ–PKAc (Fig. S4). No other AKAPs are currently known to interact at or near the N terminus of the C subunit. It is likely that PKA holoenzymes containing the fusion interact with AKAPs in a similar manner as the wild-type holoenzyme.

Because myristoylation of the PKA C subunit can effect membrane localization (21) and DnaJ is not known to be myristoylated, it is therefore likely that mis-localization of PKA occurs with the fusion. In the context of FL-HCC, however, a mechanism contributing to disease that stems from loss of myristoylation seems unlikely after further consideration. Phenotypic convergence occurs in tumors through genetic heterogeneity (22); thus, if the loss of PKAc myristoylation were the fundamental mechanistic factor contributing to FL-HCC pathogenesis, one might expect similar phenotypes from alternative, less complex myristoylation-abolishing gene defects (e.g., single point mutations or deletions restricted to the first exon of *PRKACA*). No such mutations have been found in FL-HCC patients (12, 13). Considering that PKAc Δexon1 retains full catalytic activity (Fig. S1), there may be less-selective pressure to preserve a fully intact N terminus in the C subunit and such defects would be expected were de-myristoylation the mechanism used. In Cushing's syndrome, the genetic heterogeneity found in disease tissue extends beyond defects in *PRKACA* (8) and includes numerous defects in other genes (e.g., *PRKAR1A*, *PDE11A*, and *PDE8B*), which independently may lead to disease from up-regulation of PKA activity (23). In FL-HCC, conversely, only a recurring ∼400-kb deletion in chromosome 19 was found consistently (12, 13), and this alone may represent the underlying mechanism of disease.

Disease-Causing Mutational Activation of PKA by Distinctly Different Molecular Mechanisms. Both RNA transcript and protein levels are significantly higher for the DnaJ–PKAc chimera than for wild-type PKAc, which is because of expression being placed under control of the *DNAJB1* promoter (12). RNA-Seq data reveals elevated chimeric transcript levels (3.0- to 9.2-fold increase) (Fig. S5), which is consistent with previous observations (12, 13) and leads to increased protein expression (figure 3 and figure S1 of ref. 12). The resulting up-regulation of PKA signaling coupled with a measured elevated intrinsic activity (Fig. S1) may together represent the mechanism that contributes to FL-HCC tumor pathogenesis. Gene fusions and chromosome translocations that alter promoter elements controlling oncogene expression are documented contributing factors to carcinogenesis and disease (24, 25). Overexpression of the PKA C subunit indeed contributes to disease, as discovered with copy-number gains for *PRKACA* in some cases of adrenal hyperplasia (8). In FL-HCC, a significant increase in C-subunit levels may favor formation of additional type-I holoenzyme complexes as increases in levels of RI, but not RII, are known to compensate for increased C-subunit levels (26). In the context of cancer, type I rather than type II holoenzymes are known to be associated with growth stimulation (27). In addition, if C-subunit levels overwhelm the ability to maintain equimolar ratios of R subunits normally found in healthy tissue (28), increased cAMP-independent signaling may also arise.

Both Cushing's syndrome and FL-HCC are associated with increased PKA activity, but these increases stem from different underlying molecular mechanisms. The total loss of R-subunit binding by PKAc L205R in Cushing's syndrome leads to constitutive PKA signaling, whereas much of the increased signaling from the FL-HCC fusion protein may be acute and sudden, as overexpression of the fusion from a more active promoter generates elevated levels of the cAMP-dependent holoenzyme. These resulting differences in PKA signaling between the two diseases may in part lead to the differing manifestations of disease, but differences in cellular environment likely has a significant contribution.

ATP-analog kinase inhibitors (29, 30), which bind near the active site of the PKA C subunit, may be effective in treating both diseases. Differences at the active site of the PKAc L205R mutant might be exploited for designing mutant-specific small-molecule inhibitors and new pockets formed in the fusion protein may provide options for novel disease-specific allosteric inhibitors. The results of this study, which elucidates the underlying

Downloaded from https://www.pnas.org by 174.168.116.9 on January 19, 2024 from IP address 174.168.116.9.

mechanisms of two seemingly different diseases, may guide the design of effective treatment strategies.

Materials and Methods

Cloning. Using appropriate oligonucleotide primers, DNA fragments were amplified from the appropriate sources (Table S3) by PCR and inserted into appropriate expression vectors. Residue boundaries (processed protein numbering) of all cloned constructs, expression vectors, and purification tags used in this work are summarized in Table S4. Full-length RIα and RIIβ were inserted into a modified pMCSG9 (31) vector and the rest were inserted into pLATE11 (Thermo Scientific). The four PKA catalytic subunits (PKAc, PKAc Δexon1, PKAc L205R, and DNAJ–PKAc) and the two truncated regulatory subunits in which the dimerization domain was deleted (RIα ΔDD and RIIβ ΔDD) were amplified using oligonucleotide primers that added a decahistidine purification tag (His_{10}) and a tobacco etch virus (TEV) protease cleavage site fused to the N terminus. Cloning of RIα and RIIβ into pMCSG9 fused them with a decahistidine-tagged maltose binding-protein (His_{10}MBP) at the N terminus that could be cleaved using TEV protease. The DNA fragment coding for DnaJ–PKAc was assembled using PCR and appropriate primers to fuse together two separate overlapping fragments, one derived from *DNAJB1* and the other from *PRKACA*. PKAc and DnaJ–PKAc were designed such that the remaining glycine residue left after TEV cleavage became the first glycine in the processed protein sequence. AKIP1a was engineered with a N-terminal decahistidine-tagged small ubiquitin-like modifier (His_{10}SUMO) fused to the N terminus of AKIP1a using PCR. The construct also contained a TEV protease cleavage site between His_{10}SUMO and AKIP1a, which left an additional glycine reside at the N terminus after cleavage.

Protein Expression and Purification. All expression vectors were transformed into *Escherichia coli* Rosetta 2 (DE3) cells (EMD Millipore) and all proteins were expressed by the autoinduction method (32) using media supplemented with 100 μg/mL carbenicillin. Initial noninducing starter cultures were grown at 37 °C in shaking flasks containing PAG media overnight, then diluted 100-fold into glass bottles containing 2 L of PA-5052 autoinduction media the next day. Using a LEX bioreactor system (Harbinger Biotechnology and Engineering), the cultures were aerated at 37 °C until noticeably turbid (~3–4 h), after which the temperature was lowered to 25 °C for autoinduction overnight for ~16 h. Cells were pelleted by centrifugation, resuspended in binding buffer (20 mM Hepes, pH 7.8, 500 mM NaCl, and 25 mM imidazole), and lysed by sonication. All catalytic and regulatory subunit constructs were expressed in the soluble fraction. Supernatant was cleared by centrifugation and proteins were purified by two-step nickel-affinity/gel filtration (1 mL HiTrap chelating, HP/HiLoad 16/60 Superdex columns) chromatography using the AKTAxpress system (GE Healthcare). The nickel-affinity elution buffer was identical to the binding buffer except the concentration of imidazole was increased to 0.5 M, and the gel-filtration buffer consisted of 20 mM Hepes pH 7.8, 0.15M NaCl, 20 mM imidazole, and 0.3 mM Tris(2-carboxyethyl)phosphine hydrochloride (TCEP). Where necessary, purification tags were removed using TEV-protease (33) after which the cleaved tag and the protease were removed using Ni-nitrilotriacetic acid (Ni-NTA) Agarose (Quiagen).

Catalytic subunits used for crystallization were further purified by ion-exchange chromatography (MonoS 5/50 GL) using an AKTA FPLC system. After purification tag removal, the proteins were diluted threefold using 20 mM 2-(*N*-morpholino)ethanesulfonic acid (Mes) pH 6.5 to lower the ionic strength before injection onto the column, and a KCl gradient up to 300 mM in the same buffer was used for elution. Pooled fractions of the predominant peak were dialyzed into a buffer containing 25 mM Tris pH 7.5 and 25 mM NaCl before crystallization. Preparations of some proteins contained a mixture of phosphorylation states, which were difficult to resolve. Structure determination revealed that PKAc L205R was partially autophosphorylated at Ser139 and Ser338 but fully autophosphorylated at Thr197. DnaJ–PKAc was fully autophosphorylated at Thr252 (corresponds with Thr197 in PKAc) and Ser393 (corresponds with Ser338 in PKAc) but partially autophosphorylated at Ser194 (corresponds with Ser139 in PKAc). On the other hand, PKAc and PKAc Δexon1 were fully autophosphorylated at Ser139, Thr197, and Ser338.

Purification of AKIP1a required refolding from inclusion bodies. Following cell lysis and centrifugation, the insoluble fraction was washed once with 50 mM Tris pH 8.0, 0.5 M NaCl, and 1% Triton X-100 and twice with 25 mM Tris pH 8.0, 150 mM NaCl, and 1 mM EDTA. Inclusion body paste (~0.18 g) was dissolved in 10 mL of 8 M urea, 25 mM Tris pH 8.0, 150 mM NaCl, and 2 mM DTT at room temperature. Following centrifugation to remove insoluble particles, the mixture was diluted to a final volume of 100 mL in the same buffer with lower urea concentration of 6 M. Urea was removed by dialysis at 4 °C against a buffer containing 25 mM Tris pH 8.0 and 150 mM NaCl. Protein precipitates were removed by centrifugation, imidazole was added to 25 mM, and protein was purified using the AKTAexpress system as previously described. Protein eluting from the gel filtration column as a monomeric peak of molecular weight corresponding to that of His_{10}-SUMO-AKIP1a was pooled. As necessary, the His_{10}-SUMO purification tag could be removed from AKIP1a using TEV-protease in the same manner, as previously described.

Crystallization and Data Collection. PKAc, PKAc Δexon1, PKAc L205R, and DnaJ–PKAc were concentrated to ~16 mg/mL and supplemented with magnesium chloride, ATP, and the PKI(5–24) peptide (Promega) at concentrations of 2.5 mM, 5 mM, and 0.6 mM, respectively, before crystallization. All crystals grew within a week by the sitting-drop vapor diffusion method in trays incubated at 4 °C in which 0.2–0.35 nL of protein solution was mixed with an equal volume of crystallization buffer per well. Crystals of PKAc were grown from a condition containing 10% (wt/vol) polyethylene glycol (PEG) 6000 and 0.1 M Hepes pH 7.5. Crystals of PKAc Δexon1 and PKAc L205R were grown from a condition containing 10% (wt/vol) PEG 8000 and 0.1 M Hepes pH 7.5. Crystals of DnaJ–PKAc were grown in a condition containing 0.07 M sodium cacodylate pH 6.5, 0.15 M magnesium acetate, 0.02 M zinc chloride, 5% (vol/vol) glycerol, and 11.5% (wt/vol) PEG 8000.

All crystals were flash-frozen in liquid nitrogen after a brief soak in a cryoprotectant solution identical to the crystallization buffer with the added ligands, supplemented with 20% (vol/vol) ethylene glycol. For all structures, data were collected from a single crystal at the X4C beamline at the National Synchrotron Light Source of Brookhaven National Laboratory.

Structure Determination and Refinement. HKL2000 (34) and CCP4 (35) were used for indexing and merging of data. PHENIX (36) and COOT (37) were used for refinement and model building. Phaser (38) was used for molecular replacement. The structure of PKAc Δexon1 was solved by refinement against a high-resolution structure of a PKA catalytic subunit in complex with PKI(5–24) (PDB ID code: 2GFC), which crystallized in the same space-group with similar unit cell parameters as PKAc Δexon1. The structure of PKAc and PKAc L205R was solved using the refined structure of PKAc Δexon1 as a molecular replacement search model. The structure of DnaJ–PKAc was solved using the refined structure of PKAc Δexon1 and residues 5–70 of *Thermus thermophilus* DnaJ (PDB ID code 4J7Z) as molecular replacement search models. A cross-validation test set was created from a random 5% of the reflections. All models were manually rebuilt with ligands added as necessary, and refined iteratively until convergence. The locations of all zinc atoms in the DnaJ–PKAc structure, necessary for greatly improved crystal quality, were verified by inspection of anomalous difference Fourier maps.

PKA Activity Assays. Kinase activities of PKAc, PKAc Δexon1, PKAc L205R, and DnaJ–PKAc (purification tags removed) were measured using the Universal Kinase Activity Kit (RnD Systems) that is based on a phosphatase-coupled method (39). Protein samples from two independent protein preparations were dialyzed overnight into buffer containing 25 mM Tris pH 7.5 and 0.15 M NaCl. Protein concentrations were determined in triplicate by spectrophotometry (λ = 280 nm) using a NanoDrop 2000 spectrophotometer (Thermo Scientific). Following the manufacturer's protocol, a range of appropriate dilutions of protein were incubated at room temperature for 10 min in 50-μL reaction volumes of assay buffer (25 mM Hepes pH 7.0, 0.15 M NaCl, 10 mM $MgCl_2$, and 10 mM $CaCl_2$) containing 0.1-μg coupling phosphatase and 0.2 mM ATP, both supplied in the kit. Kemptide peptide (Sigma-Aldrich) of sequence LRRASLG was added in each reaction to 0.4 mM to serve as the phospho-acceptor substrate. Following quantitation of inorganic phosphate released from kinase-generated ADP by the coupling phosphatase, using reagents supplied in the kit and referencing a phosphate standard curve, kinase activity was calculated using the appropriate coupling rate of 0.475. Average kinase activities in units of picomole of transferred phosphate per min/pmol of kinase were determined from replicate measurements.

Gel-Filtration Analysis of R-C Heterodimers and Heterotetramers. The interaction between R and C subunits (all purification tags removed) in solution was determined by gel-filtration chromatography. To determine formation of heterodimers, either PKAc L205R or DnaJ–PKAc were mixed with either RIα ΔDD or RIIβ ΔDD, each at final concentrations of 42 μM in 200 μL of buffer, and coinjected injected onto a Superdex 200 10/300 GL column (GE Healthcare) at 4 °C with a flow rate of 0.5 mL/min. Absorbance curves at a wavelength of 280 nm were recorded and compared with curves generated by injections of each alone. As a control, purified wild-type PKAc was used in place of mutant C subunits. Protein molecular weight standards (GE Healthcare) were injected for reference. Heterotetramer formation between

Downloaded from https://www.pnas.org by 174.168.116.9 on January 19, 2024 from IP address 174.168.116.9.

DnaJ–PKAc with either RIα or RIIβ was determined in the same manner. The buffer contained 25 mM Tris pH 7.5, 150 mM NaCl, 5 mM β-mercaptoethanol, 1 mM ATP, and 2 mM $MgCl_2$ for experiments with type I R subunits, and ATP and $MgCl_2$ omitted in experiments with type II R subunits.

R-C Subunit SPR Experiments. Binding kinetics between monomeric R subunits (RIα ΔDD and RIIβ ΔDD) and C subunits (PKAc and DnaJ–PKAc) were determined using SPR using the ProteOn protein interaction array system (Bio-Rad). PKAc and DnaJ–PKAc purified with intact His_{10} purification tags were each diluted into buffer containing 25 mM Hepes pH 7.0, 150 mM KCl, 1 mM TCEP, 0.05% Tween-20, 1 mM ATP, and 2 mM $MgCl_2$ to protein concentrations of 0.5 and 1.0 μg/mL. The C subunit were immobilized as ligands in parallel in separate channels on a nickel-activated ProteOn HTG chip at a flow rate of 30 μL/min until immobilization levels of ∼300 and ∼500 response units (RU) were reached for the lower and higher concentration samples, respectively. The R subunits (purification tags removed) were diluted into the same buffer at four different concentrations (3 nM, 1 nM, 0.33 nM, and 0.11 nM) and injected in parallel as analytes. The association and dissociation phases were monitored for 600 and 2,400 s, respectively, with a flow rate of 35 μL/min in same buffer conditions at 25 °C (the dissociation phase contained no protein in the buffer). The chip was regenerated with buffer containing 100 μM cAMP injected at 100 μL/min for 45 s. The group binding data for each set of regulatory subunit dilutions were fitted using a standard 1:1 Langmuir binding model with the ProteOn Manager software. Data fitting with additional mass-transfer correction terms showed that mass-transfer effects were minimal. Mean values and SDs were calculated from pairs of ligand–analyte interactions measured from the two immobilized ligand levels.

His-Tag Pull Downs. To reveal interactions between AKIP1a and C subunits, 25 μL of Ni-NTA agarose was incubated for 3 h at 4 °C with equimolar mixtures of purified DnaJ–PKAc or PKAc (all purification tags removed) with His_{10}SUMO-AKIP1a (intact purification tag) (typically 6–12 μg of each) in 400-μL gel-filtration buffer (20 mM Hepes pH 7.8, 0.15M NaCl, 20 mM imidazole, 0.3 mM TCEP) containing 0.05% Triton X-100. Incubations performed without His_{10}SUMO-AKIP1a were used as controls. Resins were subsequently extensively washed with buffer and proteins were eluted using SDS/PAGE loading buffer, separated by SDS/PAGE, and visualized by staining with Coomassie blue. In a similar manner, His_{10}DnaJ-PKAc (intact purification tag) was incubated with AKIP1a (tag removed).

Quantitation of *PRKACA* Expression. As previously described (12), the RNA-Seq reads were mapped to the genome with STAR (40). Gene expression was quantified with HTSeq-count and normalized with DESeq.

ACKNOWLEDGMENTS. We thank David Hirsh, Tom Maniatis, and Willa Appel for helpful discussions; Antonio Luz of the High-Throughput and Spectroscopy Resource Center at The Rockefeller University for training and assistance in the surface plasmon resonance experiments; and Randy Abramowitz for help at synchrotron beamline X4C. Beamline X4C is supported by the New York Structural Biology Center at the National Synchrotron Light Source of Brookhaven National Laboratory, a Department of Energy facility.

1. Kim C, Xuong NH, Taylor SS (2005) Crystal structure of a complex between the catalytic and regulatory (RIalpha) subunits of PKA. *Science* 307(5710):690–696.
2. Taylor SS, Buechler JA, Yonemoto W (1990) cAMP-dependent protein kinase: Framework for a diverse family of regulatory enzymes. *Annu Rev Biochem* 59:971–1005.
3. Brown SHJ, Wu J, Kim C, Alberto K, Taylor SS (2009) Novel isoform-specific interfaces revealed by PKA RIIbeta holoenzyme structures. *J Mol Biol* 393(5):1070–1082.
4. Boettcher AJ, et al. (2011) Realizing the allosteric potential of the tetrameric protein kinase A RIα holoenzyme. *Structure* 19(2):265–276.
5. Ilouz R, et al. (2012) Localization and quaternary structure of the PKA RIβ holoenzyme. *Proc Natl Acad Sci USA* 109(31):12443–12448.
6. Zhang P, et al. (2012) Structure and allostery of the PKA RIIβ tetrameric holoenzyme. *Science* 335(6069):712–716.
7. Jarnaess E, Taskén K (2007) Spatiotemporal control of cAMP signalling processes by anchored signalling complexes. *Biochem Soc Trans* 35(Pt 5):931–937.
8. Beuschlein F, et al. (2014) Constitutive activation of PKA catalytic subunit in adrenal Cushing's syndrome. *N Engl J Med* 370(11):1019–1028.
9. Goh G, et al. (2014) Recurrent activating mutation in *PRKACA* in cortisol-producing adrenal tumors. *Nat Genet* 46(6):613–617.
10. Cao Y, et al. (2014) Activating hotspot L205R mutation in *PRKACA* and adrenal Cushing's syndrome. *Science* 344(6186):913–917.
11. Sato Y, et al. (2014) Recurrent somatic mutations underlie corticotropin-independent Cushing's syndrome. *Science* 344(6186):917–920.
12. Honeyman JN, et al. (2014) Detection of a recurrent *DNAJB1-PRKACA* chimeric transcript in fibrolamellar hepatocellular carcinoma. *Science* 343(6174):1010–1014.
13. Xu L, et al. (2015) Genomic analysis of fibrolamellar hepatocellular carcinoma. *Hum Mol Genet* 24(1):50–63.
14. Zheng J, et al. (1993) Crystal structure of the catalytic subunit of cAMP-dependent protein kinase complexed with MgATP and peptide inhibitor. *Biochemistry* 32(9): 2154–2161.
15. Knighton DR, et al. (1991) Crystal structure of the catalytic subunit of cyclic adenosine monophosphate-dependent protein kinase. *Science* 253(5018):407–414.
16. Narayana N, Cox S, Shaltiel S, Taylor SS, Xuong N (1997) Crystal structure of a polyhistidine-tagged recombinant catalytic subunit of cAMP-dependent protein kinase complexed with the peptide inhibitor PKI(5-24) and adenosine. *Biochemistry* 36(15): 4438–4448.
17. Barends TRM, et al. (2013) Combining crystallography and EPR: Crystal and solution structures of the multidomain cochaperone DnaJ. *Acta Crystallogr D Biol Crystallogr* 69(Pt 8):1540–1552.
18. Wirtenberger M, et al. (2007) The functional genetic variant Ile646Val located in the kinase binding domain of the A-kinase anchoring protein 10 is associated with familial breast cancer. *Carcinogenesis* 28(2):423–426.
19. Sastri M, Barraclough DM, Carmichael PT, Taylor SS (2005) A-kinase-interacting protein localizes protein kinase A in the nucleus. *Proc Natl Acad Sci USA* 102(2):349–354.
20. Gao N, Hibi Y, Cueno M, Asamitsu K, Okamoto T (2010) A-kinase–interacting protein 1 (AKIP1) acts as a molecular determinant of PKA in NF-kappaB signaling. *J Biol Chem* 285(36):28097–28104.
21. Gaffarogullari EC, et al. (2011) A myristoyl/phosphoserine switch controls cAMP-dependent protein kinase association to membranes. *J Mol Biol* 411(4):823–836.
22. Gerlinger M, et al. (2012) Intratumor heterogeneity and branched evolution revealed by multiregion sequencing. *N Engl J Med* 366(10):883–892.
23. Almeida MQ, Stratakis CA (2011) How does cAMP/protein kinase A signaling lead to tumors in the adrenal cortex and other tissues? *Mol Cell Endocrinol* 336(1-2):162–168.
24. Croce CM, Erikson J, ar-Rushdi A, Aden D, Nishikura K (1984) Translocated c-myc oncogene of Burkitt lymphoma is transcribed in plasma cells and repressed in lymphoblastoid cells. *Proc Natl Acad Sci USA* 81(10):3170–3174.
25. Edwards PAW (2010) Fusion genes and chromosome translocations in the common epithelial cancers. *J Pathol* 220(2):244–254.
26. Uhler MD, McKnight GS (1987) Expression of cDNAs for two isoforms of the catalytic subunit of cAMP-dependent protein kinase. *J Biol Chem* 262(31):15202–15207.
27. Cho-Chung YS, Clair T (1993) The regulatory subunit of cAMP-dependent protein kinase as a target for chemotherapy of cancer and other cellular dysfunctional-related diseases. *Pharmacol Ther* 60(2):265–288.
28. Hofmann F, Bechtel PJ, Krebs EG (1977) Concentrations of cyclic AMP-dependent protein kinase subunits in various tissues. *J Biol Chem* 252(4):1441–1447.
29. Parang K, Cole PA (2002) Designing bisubstrate analog inhibitors for protein kinases. *Pharmacol Ther* 93(2-3):145–157.
30. Zhang J, Yang PL, Gray NS (2009) Targeting cancer with small molecule kinase inhibitors. *Nat Rev Cancer* 9(1):28–39.
31. Donnelly MI, et al. (2006) An expression vector tailored for large-scale, high-throughput purification of recombinant proteins. *Protein Expr Purif* 47(2):446–454.
32. Studier FW (2005) Protein production by auto-induction in high density shaking cultures. *Protein Expr Purif* 41(1):207–234.
33. Blommel PG, Fox BG (2007) A combined approach to improving large-scale production of tobacco etch virus protease. *Protein Expr Purif* 55(1):53–68.
34. Otwinowski Z, Minor W (1997) Processing of X-ray diffraction data collected in oscillation mode. *Methods Enzymol* 276:307–326.
35. Winn MD, et al. (2011) Overview of the CCP4 suite and current developments. *Acta Crystallogr D Biol Crystallogr* 67(Pt 4):235–242.
36. Adams PD, et al. (2010) PHENIX: A comprehensive Python-based system for macromolecular structure solution. *Acta Crystallogr D Biol Crystallogr* 66(Pt 2):213–221.
37. Emsley P, Lohkamp B, Scott WG, Cowtan K (2010) Features and development of Coot. *Acta Crystallogr D Biol Crystallogr* 66(Pt 4):486–501.
38. McCoy AJ, et al. (2007) Phaser crystallographic software. *J Appl Cryst* 40(Pt 4):658–674.
39. Wu ZL (2011) Phosphatase-coupled universal kinase assay and kinetics for first-order-rate coupling reaction. *PLoS ONE* 6(8):e23172.
40. Dobin A, et al. (2013) STAR: Ultrafast universal RNA-seq aligner. *Bioinformatics* 29(1): 15–21.
41. Kim C, Cheng CY, Saldanha SA, Taylor SS (2007) PKA-I holoenzyme structure reveals a mechanism for cAMP-dependent activation. *Cell* 130(6):1032–1043.

Downloaded from https://www.pnas.org by 174.168.116.9 on January 19, 2024 from IP address 174.168.116.9.